THE ASTROPHYSICAL JOURNAL, 462:89–103, 1996 May 1


# KECK SPECTROSCOPY AND *HUBBLE SPACE TELESCOPE* IMAGING OF FIELD GALAXIES AT MODERATE REDSHIFT[1,2]

DUNCAN A. FORBES, ANDREW C. PHILLIPS, DAVID C. KOO, AND GARTH D. ILLINGWORTH
Lick Observatory, University of California, Santa Cruz, CA 95064
*Received 1995 July 12; accepted 1995 November 6*

## ABSTRACT

We present 18 spectra, obtained with the Keck 10 m telescope, of faint field galaxies ($19 < I < 22$, $0.2 < z < 0.84$) previously imaged by the *Hubble Space Telescope* (*HST*) Wide Field and Planetary Camera 2 (WFPC2). Though small, our sample appears to be representative of field spirals with a magnitude limit of $I \leq 22$. Combining the results from the spectral and imaging data, we have derived various quantitative parameters for the galaxies, including colors, inclinations, emission-line equivalent widths, redshifts, luminosities, internal velocity information, and physical scale lengths. In particular, disk scale lengths (with sizes ranging from $\sim 1$ to 5 kpc) have been measured from fits to the surface brightness profiles. We have also measured internal velocities with a rest frame resolution of $\sigma = 55$–$80$ km s$^{-1}$ by fitting to the emission lines. The luminosity-disk size and luminosity–internal velocity (Tully-Fisher) relations for our moderate redshift galaxies are similar to the scaling relations seen for local galaxies, albeit with a modest brightening of $\sim 1$ mag. The one bulge-dominated galaxy in our sample (at $z = 0.324$) has a relatively blue color, reveals weak emission lines, and is $\sim 0.5$ mag brighter in the rest frame than expected for a passive local elliptical. Our data suggest that galaxies at about half the age of the universe have undergone mild luminosity evolution to the present epoch but are otherwise quantitatively similar to galaxies seen locally.

*Subject headings:* cosmology: observations — galaxies: evolution — galaxies: kinematics and dynamics — galaxies: photometry — galaxies: spiral — galaxies: structure

## 1. INTRODUCTION

The nature and evolution of galaxies is an active research area in contemporary astronomy. Considerable telescope time has been spent pursuing this topic, yet it is still the subject of much debate largely because of the observational difficulties involved in collecting large, unbiased data sets of galaxies at faint magnitudes and the lack of comparable local samples. The bulk of research has focused on number counts (to around $B \sim 26$), redshift distributions (to $B \sim 24$), clustering properties, and integrated colors (e.g., Koo & Kron 1992; Lilly et al. 1995). A few ground-based studies of the morphology of distant galaxies (to $B \sim 24$) have been attempted (e.g., Lavery, Pierce, & McClure 1992; Giraud 1992), but these are limited to spatial resolutions of $\geq 0\farcs5$. Clear advances in this area have been made by the *Hubble Space Telescope* (*HST*) using the first Wide Field and Planetary Camera (e.g., Dressler et al. 1994a; Griffiths et al. 1994a; Couch et al. 1994; Phillips et al. 1995a) and recently with the much improved WFPC2 (Dressler et al. 1994b; Forbes et al. 1994; Griffiths et al. 1994b; Cowie, Hu, & Songaila 1995). Imaging with the *HST* allows morphological and structural information on subkiloparsec-size scales to be determined for distant galaxies.

An important tool for studying nearby galaxies via their internal kinematics is the Faber-Jackson relation for elliptical galaxies (Faber & Jackson 1976) and the Tully-Fisher relation for spiral galaxies (Tully & Fisher 1977). So far, there are only a handful of galaxies with redshifts greater than 0.1 for which internal velocity measurements have been published. Franx (1993a, b) derived internal velocity information for several galaxies in the cluster A665 ($z = 0.18$). At a slightly higher redshift ($z \sim 0.2$) Vogt et al. (1993) measured a full rotation curve for field two spiral galaxies. Kinematic information on more distant galaxies would provide a powerful diagnostic of internal dynamics and allow galaxy evolution to be traced by mass as distinct from light.

Here we present a small data set from which we examine internal kinematics and sizes for galaxies at moderate redshift ($0.2 < z < 0.84$). Our data consist of 18 field galaxies with $I$-band magnitudes between 19 and 22 ($\sim 20.5 < B < 24.5$), for which we have high spatial resolution imaging from the WFPC2 camera of *HST* and moderate-resolution spectra obtained on the Keck 10 m telescope. These galaxies were originally selected from field galaxies in Medium Deep Survey (MDS) images (Griffiths et al. 1994a; Forbes et al. 1994). The images and spectra allow us to derive redshifts, velocity information, equivalent widths, Hubble classifications, inclinations, colors, and physical scale lengths for these galaxies.

The median redshift of our sample ($\bar{z} = 0.48$) corresponds to a look-back time that is about half the age of the universe and for which some scenarios predict significant evolution in galaxy populations (for a review, see Koo & Kron 1992). Of particular interest are the "faint blue galaxies" that appear to dominate the number counts of field galaxies, with a factor of 3–5 above no-evolution predictions, by $B \sim 23$ (e.g., Cowie, Songaila, & Hu 1991). It has been suggested that these galaxies may have faded by several magnitudes (e.g., Cowie et al. 1991) or merged (e.g., Broadhurst, Ellis, & Glazebrook 1992), so that they have "disappeared"

[1] Based on observations with the NASA/ESA *Hubble Space Telescope*, obtained at the Space Telescope Science Institute, which is operated by AURA, Inc., under NASA contract NAS 5-26555.

[2] Based on observations obtained at the W. M. Keck Observatory, which is operated jointly by the California Institute of Technology and the University of California.

by the present epoch and thus do not have local counterparts. Our main result from this work, after comparing the size and internal kinematics with luminosity to those of local galaxies, is that *a sample of representative disk galaxies up to half the age of the universe has undergone only a modest amount* ($\sim 1$ mag) *of luminosity evolution.* We assume $H_0 = 75$ km s$^{-1}$ Mpc$^{-1}$ and $q_0 = 0$ throughout this paper.

## 2. OBSERVATIONS AND DATA REDUCTION

The galaxies described in this paper come from three high galactic latitude MDS WFPC2 fields, called MDS U1, U5, and U54. The first two fields were studied by Forbes et al. (1994), who classified over 200 field galaxies according to their morphological type and derived total $I$-band magnitudes. The field MDS U54 consists of 3 × 1800 s F606W ($V$) band and 3 × 1200 s F814W ($I$) band images observed on 1994 July 4. These data were reduced, combined, and calibrated in a manner similar to that described in Forbes et al. (1994). A mosaic of the WFPC2 galaxy images is given in Figure 1 (Plate 6), and a summary of the measurements from the imaging data is presented in Table 1.

The galaxies selected for follow-up spectroscopy were chosen so that two would lie on a single long slit. They were not picked to have a particular morphology or angular size. For one galaxy in our sample (number 3), the redshift was known from the work of Glazebrook et al. (1994), but its nature (super-starburst or gravitational lens) as discussed by Glazebrook et al. was uncertain. A discussion of whether our galaxies are typical of those expected in an $I < 22$ magnitude-limited sample is given in § 4.1. The spectroscopic data were obtained during 1994 September 8–10 using the W. M. Keck 10 m telescope on Mauna Kea, Hawaii. We used the Low Resolution Imaging Spectrograph (LRIS; Oke et al. 1995) in long-slit mode with a 1″.0 wide slit. The spectral dispersion was 1.28 Å pixel$^{-1}$ and the spatial scale was 0″.22 pixel$^{-1}$. The data were obtained under FWHM $\sim$ 0″.8 seeing conditions and partial clouds. After locating the galaxies in the slit-guiding camera, the slit was placed so as to obtain spectra of at least two galaxies. A typical integration was a single 1800 s exposure (see Table 2 for details), covering 4700–7300 Å. The FWHM instrumental resolution is $R \sim 1300$, which corresponds to a rest frame instrumental velocity ($\sigma$ = FWHM/2.35) of 55–80 km s$^{-1}$ for our sample galaxies.

The data were reduced using the IRAF package. The bias was removed and the data corrected for the amplifier gain between the two halves of the CCD. Several dome exposures, illuminated by a quartz lamp, were combined and fitted using a low-order polynomial. In the absence of suitable sky frames, this traces the response across the slit (low spatial frequency variations). After dividing by the polynomial fit, we created a "dome flat" which was used to correct for pixel-to-pixel variations to the few percent level. The spectrum centroid and S-distortion were traced out using the APALL task. This task was also used to define the sky region near the spectrum. Geometric distortion along the wavelength direction was found to be very small (<0.1 pixels) for most of our data. Tests on the most extreme cases showed that correcting for this small distortion had no effect on the redshift determination or width of the emission lines within our measurement errors (further discussion of errors is given below). After subtracting sky, from regions typically 20 pixels wide on either side of the nucleus, we wavelength calibrated using the night-sky lines. The data have not been flux calibrated. A total of 18 galaxy spectra have been extracted.

## 3. RESULTS

### 3.1. *HST Imaging*

We have fitted elliptical isophotes to the galaxy images using the same method as Phillips et al. (1995a, b). From this modeling, we measure the axial ratio of the outer isophotes, position angle on the sky, and a surface brightness

TABLE 1

*HST* IMAGING

| Identification Number (1) | Galaxy Name (2) | $V$, $I$ Exposure Times (3) | Hubble Type (4) | Structure (5) | $I$ total (mag) (6) | $V-I$ Color (mag) (7) | Axial Ratio (8) |
|---|---|---|---|---|---|---|---|
| 1..... | 030505.0−001143 | 2400, 6600 | Sb | ... | 19.7 | 1.15 | 0.92 |
| 2..... | 030504.9−001138 | 2400, 6600 | Irr | ... | 21.9 | 1.00 | 0.63 |
| 3..... | 030501.3−001039 | 2400, 6600 | d | asym | 21.5 | 0.91 | 0.83 |
| 4..... | 030458.0−001135 | 2400, 6600 | ... | d.n. | 20.3 | 0.99 | 0.58 |
| 5..... | 030459.2−001146 | 2400, 6600 | Sb | ... | 19.1 | 1.23 | 0.71 |
| 6..... | 030503.4−001010 | 2400, 6600 | SBc | asym | 20.2 | 1.64 | 0.58 |
| 7..... | 030503.3−001015 | 2400, 6600 | i | ... | 21.6 | 1.22 | 0.86 |
| 8..... | 010958.5−022724 | 3300, 6300 | Sb | asym | 19.7 | 0.90 | 0.67 |
| 9..... | 010958.1−022740 | 3300, 6300 | ... | d.n. | 20.2 | 0.72 | 0.48 |
| 10 ..... | 010957.4−022807 | 3300, 6300 | Sc | asym | 19.9 | 0.68 | 0.50 |
| 11 ..... | 171220.8+333559 | 5400, 6300 | i | asym | 21.4 | 1.07 | 0.62 |
| 12 ..... | 171221.4+333556 | 5400, 6300 | Sb | asym | 19.1 | 0.68 | 0.76 |
| 13 ..... | 171227.1+333549 | 5400, 6300 | d | asym | 20.6 | 1.18 | 0.62 |
| 14 ..... | 171227.0+333558 | 5400, 6300 | i | ... | 21.1 | 0.86 | 0.60 |
| 15 ..... | 171229.5+333626 | 5400, 6300 | Sc | ... | 20.8 | 0.85 | 0.55 |
| 16 ..... | 171229.5+333634 | 5400, 6300 | SBc | asym | 20.8 | 1.41 | 0.53 |
| 17 ..... | 171229.3+333636 | 5400, 6300 | E | asym | 19.4 | 0.92 | 0.80 |
| 18 ..... | 171229.9+333644 | 5400, 6300 | Sb | asym | 20.4 | 1.02 | 0.90 |

NOTES.—Col. (1): galaxy identification number; col. (2): galaxy name (J2000 coordinate); col. (3): exposure times; col. (4): Hubble type (d = disk-dominated, i = intermediate); col. (5): visual structure (asym = asymmetric, d.n. = double nucleus); col. (6) total $I$-band magnitude (error = 0.1 mag); col. (7): total $V-I$ color (error = 0.15 mag); col. (8): axial ratio (b/a) of outer isophote (error $\sim$10%).

PLATE 6

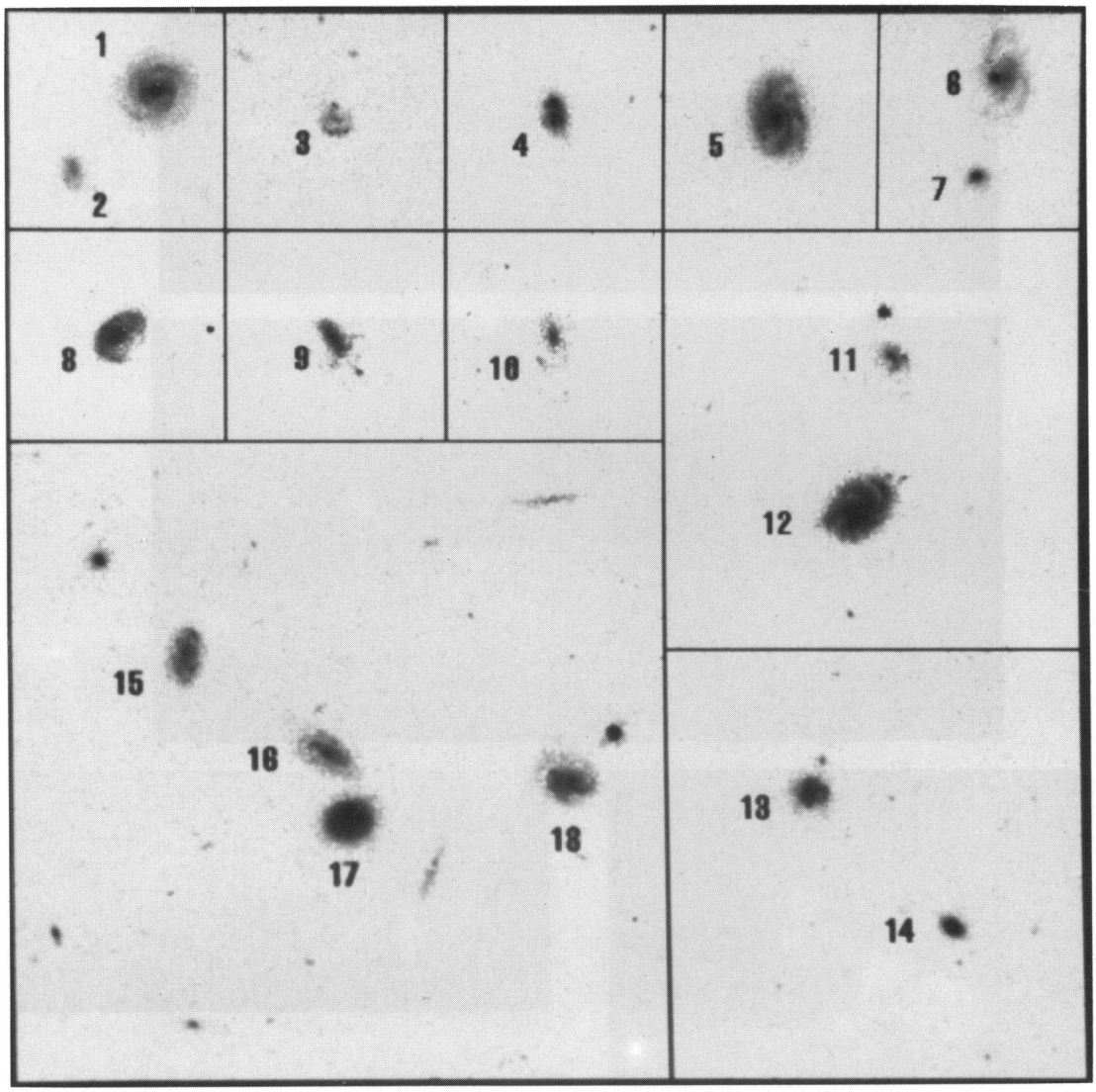


FIG. 1.—Gray-scale mosaic of the WFPC2 images of our galaxy sample. The display is logarithmic. Each subimage box has the same scale, with the small boxes being 100 pixels (10″) on a side. The galaxies are numbered as in the tables.

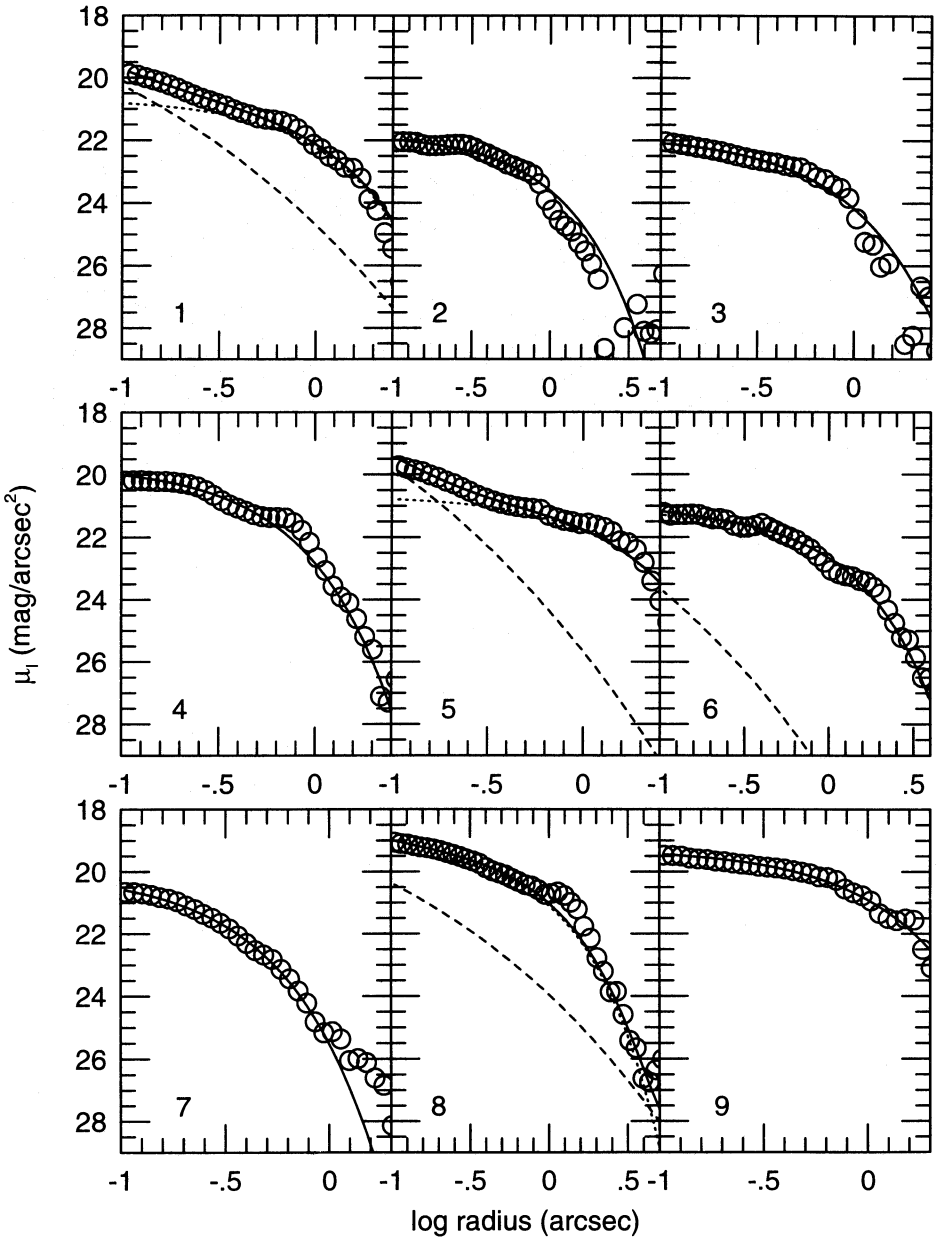


FIG. 2a

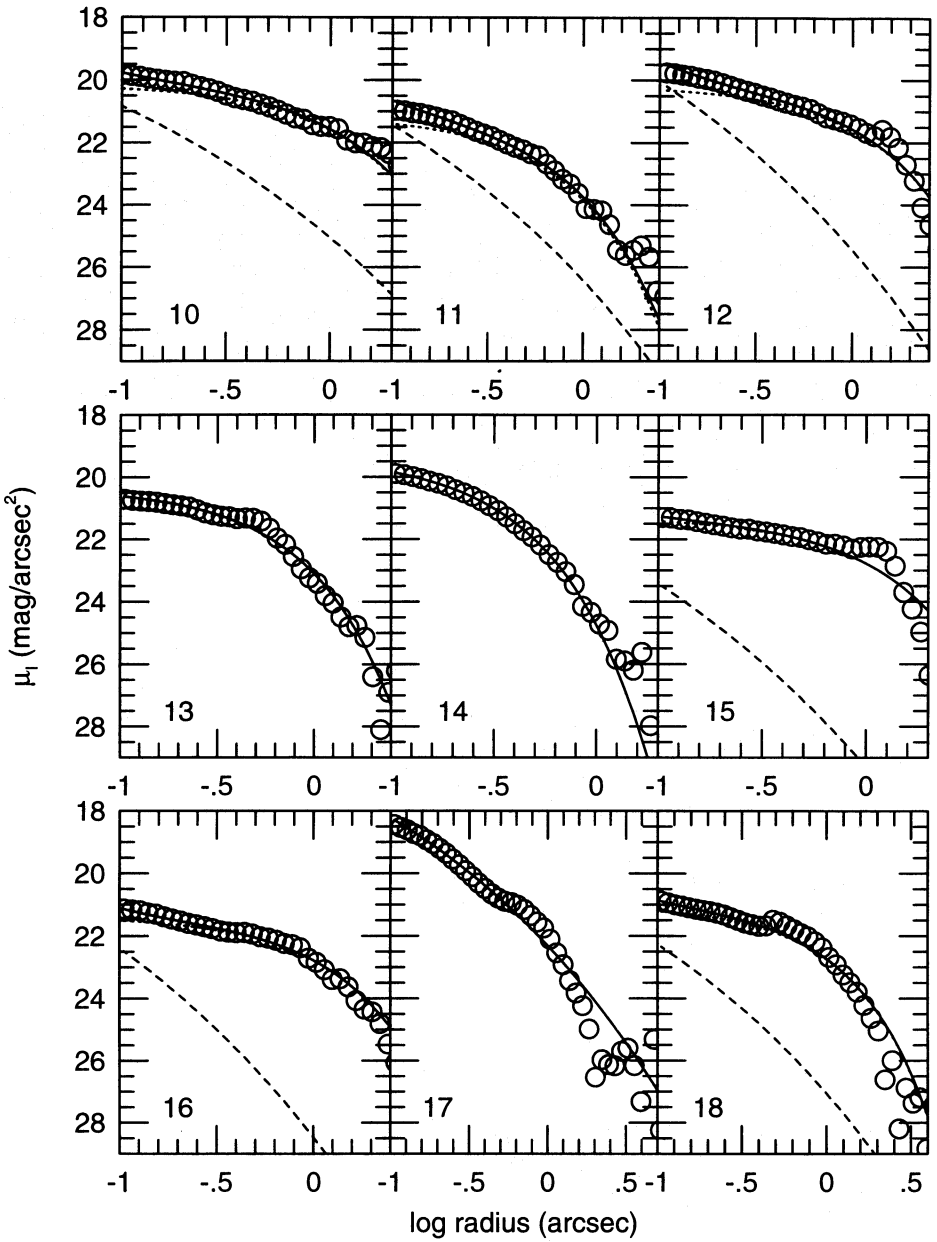


FIG. 2b

FIG. 2.—(*a*) Galaxy surface brightness profiles in the *I* band. We show the $r^{1/4}$ bulge (*dashed line*), exponential disk (*dotted line*), and combined fit (*solid line*) to each profile. The galaxies are numbered as in the tables.

profile. The major axis profile is then fitted with an $r^{1/4}$ law and/or an exponential disk profile simultaneously to give scale lengths and surface brightnesses. Surface brightness profile fits for our sample are shown in Figure 2. The galaxy morphology is classified according to the system of Forbes et al. (1994), i.e., we assign Hubble types where possible or "b" for bulge-dominated, "i" for intermediate, and "d" for disk-dominated systems (given in Table 1). This division correlates strongly with apparent magnitude, so that galaxies with $I < 21$ can generally be assigned familiar Hubble types, while those fainter are classified more crudely. In this paper we have amended the Forbes et al. (1994) morphological type of one galaxy (number 7) from "b" to "i" because we feel that this is a more accurate description of the visual morphology. For each galaxy, we have also noted any peculiar visual structure, such as a double nucleus or any asymmetries that may be caused by a merger or interaction. On this basis, there appear to be several galaxies with physical associations (see Table 1 and § 4.4).

### 3.2. *Keck Spectroscopy*

For 17 of the 18 spectra, we have derived redshifts from both emission and absorption lines. In Figure 3 we show each galaxy spectrum, smoothed to the instrumental resolution, and the location of identified lines. The measured redshifts for the galaxies lie within a range of $z = 0.205$ to $z = 0.837$, with random errors given by the rms variation from the individual lines (see Table 2). We also assign a "quality class" which indicates the reliability of the quoted redshift, with quality class A (very secure redshift) given to 13 spectra, quality B (less secure, but deserves a high weighting) given to three, quality C (marginal redshift, should be given a low weighting) given to one spectrum, and quality D (no redshift determined) given to one spectrum.

The strong emission lines have been fitted with a single Gaussian profile for H$\beta$ and [O III] $\lambda$5007 and a double Gaussian profile for the [O II] $\lambda\lambda$3726, 3729 doublet (with

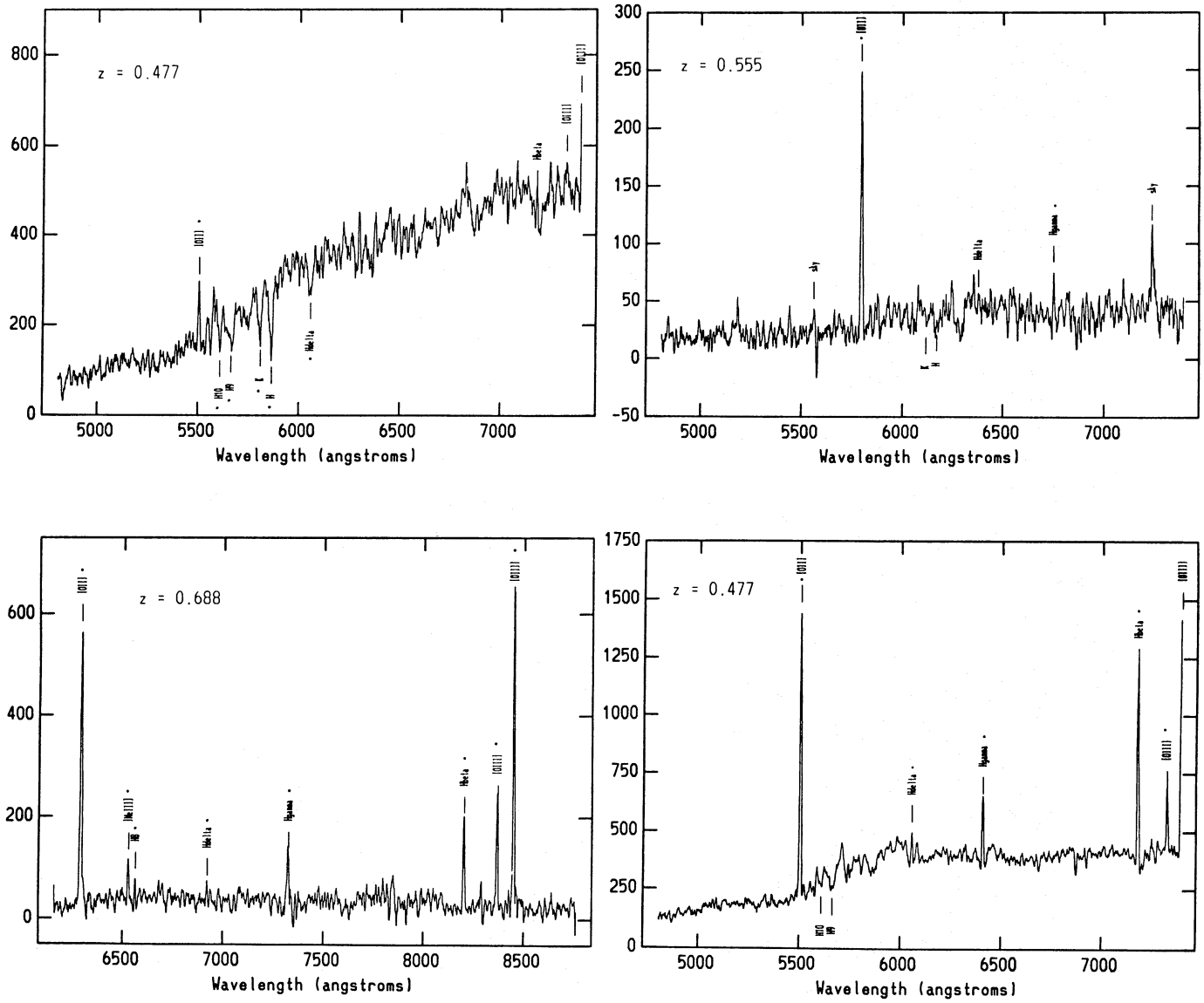


FIG. 3.—Spectra of our sample of 18 faint ($I < 22$) field galaxies. Each spectrum has been smoothed to the instrumental resolution and has the derived redshift labeled in the upper left (see Table 2). Lines used in the redshift determination are denoted by a black dot. Relative counts are given on the $y$-axis (the spectra are not flux calibrated).

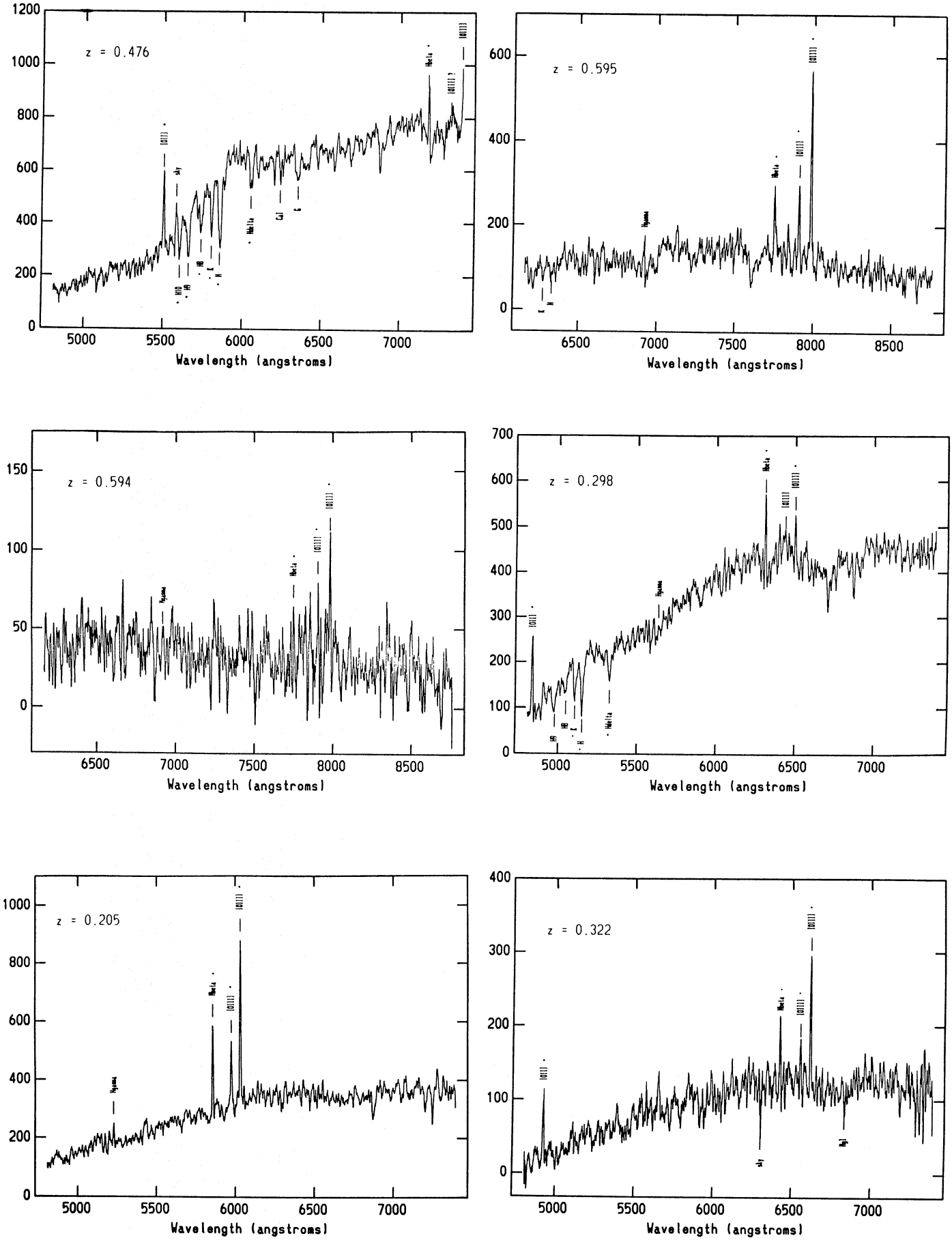


FIG. 3.—*Continued*

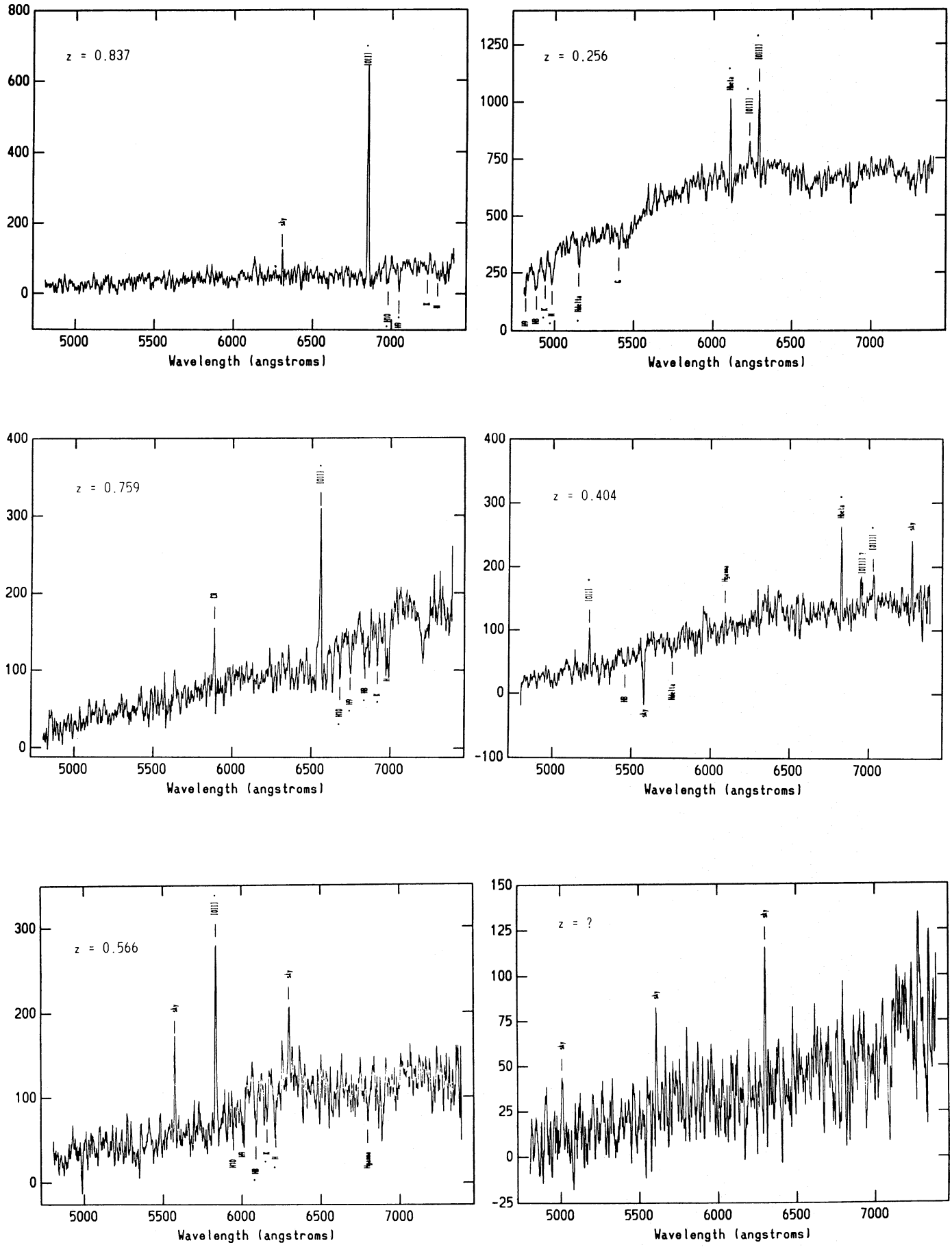


FIG. 3.—*Continued*

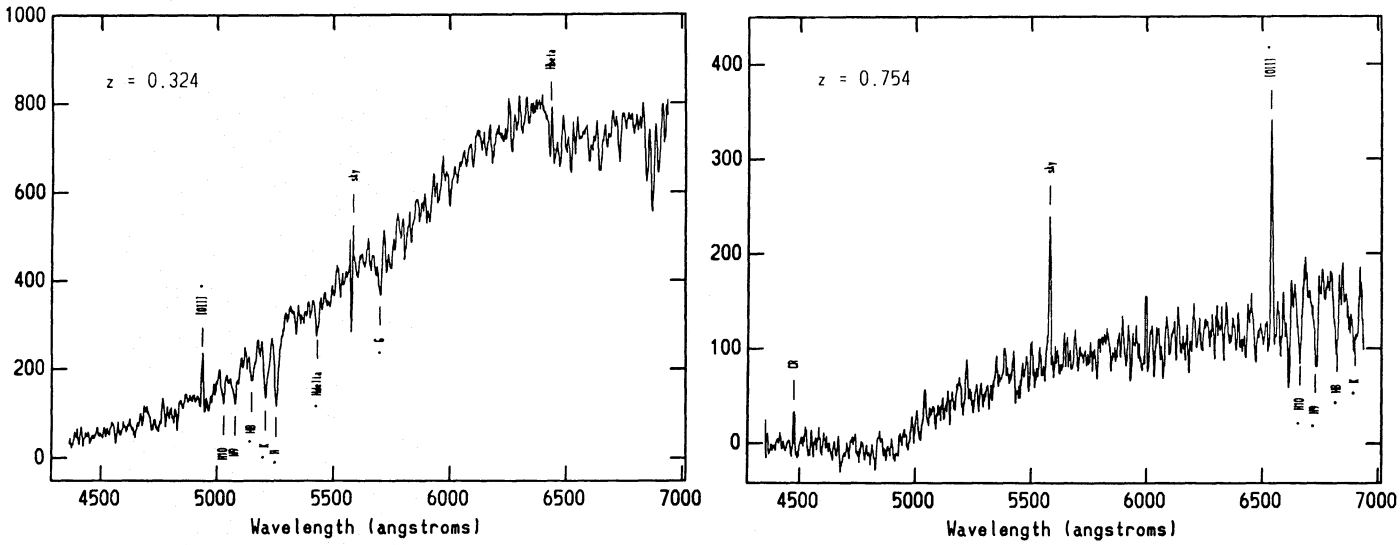


FIG. 3.—*Continued*

amplitudes allowed to vary, and a fixed rest-frame separation of 2.75 Å). An example of a Gaussian fit to Hβ and [O III] for the Sb galaxy number 12 is given in Figure 4. We have also fitted the nonblended sky lines at similar wavelengths to the emission lines with single Gaussians in order to derive the appropriate instrumental broadening. The observed emission-line FWHM, after subtracting in quadrature the instrumental profile, is given in Table 2. For the unresolved lines, we give upper limits to the galaxy's internal velocity, of FWHM equal to 120 or 200 km $s^{-1}$. These limits were chosen after smoothing various high and low signal-to-noise ratio (S/N) emission lines by a prescribed amount and then determining the level of broadening that was readily detectable. The main source of error in the FWHM determination is the quality of the Gaussian fit, which is typically ~25% based on differences in the individual emission-line fits. For the equivalent width, it is the continuum level (error ~35%). For 10 galaxies we were able to measure the velocity broadening, whereas for the others we quote upper limits. The equivalent width of the [O II] line was measured for 13 galaxies. The measured FWHM line width (corrected for instrumental broadening)

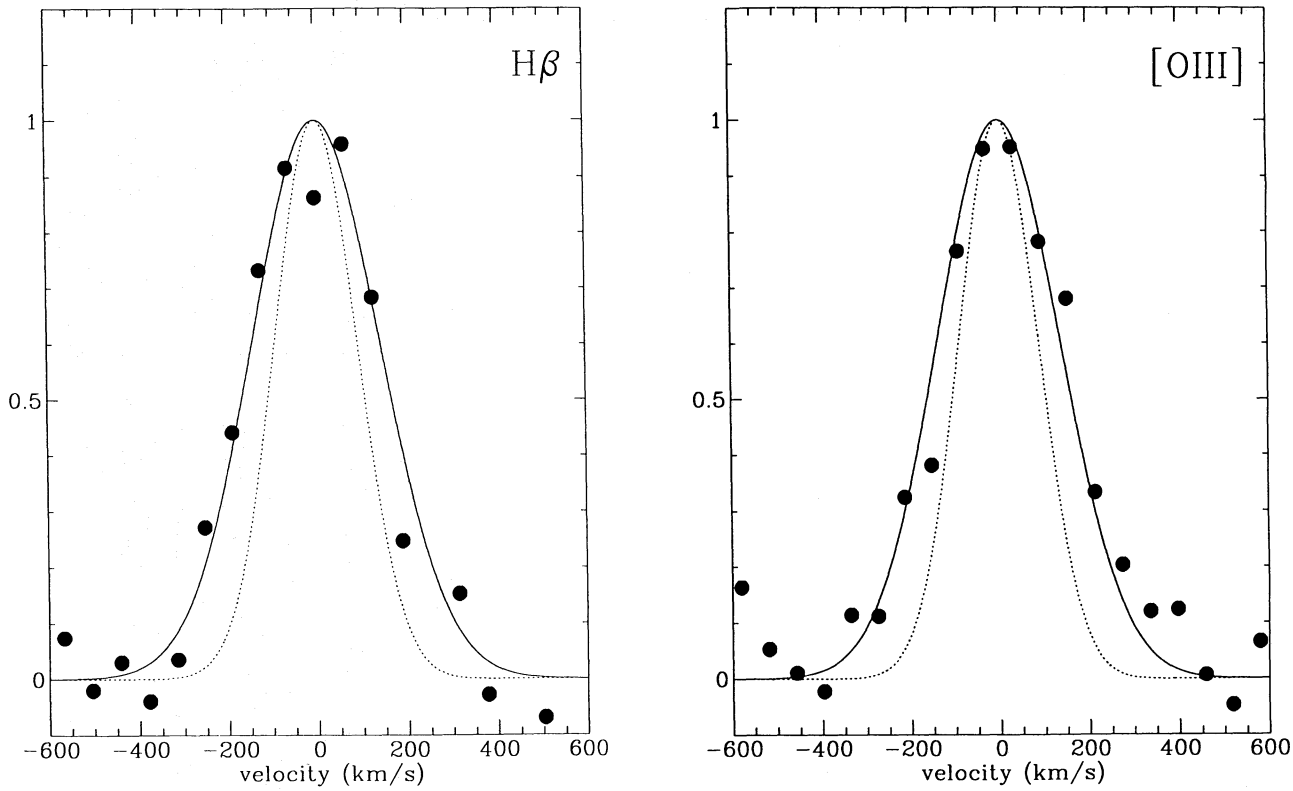


FIG. 4.—Velocity line profiles for (*a*) Hβ and (*b*) [O III] λ5007. The data for the Sb galaxy number 12 ($M_B = -20.1$, $z = 0.256$) are shown by filled circles. The same broadened Gaussian is represented by a solid line for both the Hβ and [O III] line profiles. The instrumental profile is represented by a dotted line. After correcting for the instrumental profile in quadrature, the FWHM = 247 km $s^{-1}$.

TABLE 2

KECK SPECTROSCOPY

| Identification Number (1) | Exposure Times (s) (2) | Redshift (3) | Lines (4) | Quality (5) | FWHM (km s$^{-1}$) (6) | [O II] EW$_{obs}$ (Å) (7) |
|---|---|---|---|---|---|---|
| 1..... | 1 × 1800 | 0.477 ± 0.001 | 6 | A | 160 | 11 |
| 2..... | 1 × 1800 | 0.555 ± 0.001 | 2 | B | 229 | 150 |
| 3..... | 1 × 1800 | 0.688 ± 0.001 | 8 | A | <120 | 150 |
| 4..... | 2 × 1800 | 0.477 ± 0.001 | 5 | A | 207 | 70 |
| 5..... | 2 × 1800 | 0.476 ± 0.001 | 8 | A | 234 | 13 |
| 6..... | 1 × 1350 | 0.595 ± 0.001 | 3 | A | <120 | ... |
| 7..... | 1 × 1350 | 0.594 ± 0.001 | 3 | C | <200 | ... |
| 8..... | 1 × 1800 | 0.298 ± 0.001 | 6 | A | 270 | 28 |
| 9..... | 1 × 1800 | 0.205 ± 0.001 | 3 | A | 173 | ... |
| 10 ..... | 1 × 1800 | 0.322 ± 0.001 | 4 | A | <120 | 60 |
| 11 ..... | 1 × 1800 | 0.837 ± 0.001 | 3 | B | <120 | 290 |
| 12 ..... | 1 × 1800 | 0.256 ± 0.001 | 6 | A | 247 | ... |
| 13 ..... | 1 × 1800 | 0.759 ± 0.001 | 5 | A | <120 | 30 |
| 14 ..... | 1 × 1800 | 0.404 ± 0.002 | 3 | B | <200 | 26 |
| 15 ..... | 1 × 1800 | 0.566 ± 0.001 | 4 | A | 150 | 49 |
| 16 ..... | 1 × 1800 | ... | ... | D | ... | ... |
| 17 ..... | 2 × 1800 | 0.324 ± 0.001 | 6 | A | 193 | 12 |
| 18 ..... | 2 × 1800 | 0.754 ± 0.001 | 5 | A | 122 | 26 |

NOTE.—Col. (1): galaxy identification number; col. (2): exposure time; col. (3): redshift and rms error; col. (4): number of lines used for redshift determination; col. (5): quality of the spectrum (A = excellent, C = poor); col. (6): average velocity width from emission lines, corrected for instrumental broadening only; col. (7): observed [O II] λ3727 equivalent width.

and the [O II] equivalent width are listed in Table 2 (they are not corrected for inclination or redshift).

### 3.3. *Derived Parameters*

Combining results from the spectral and imaging data, we have derived several physical parameters for our sample galaxies (see Table 3). In column (1) we give the Galaxy identification number. Columns (2) and (3) give the physical scale and absolute $B$ magnitude ($M_B$) assuming $H_0 = 75$ km s$^{-1}$ Mpc$^{-1}$ and $q_0 = 0$. The absolute magnitude at zero redshift is calculated using the observed color with the tables of Frei & Gunn (1994), which give $K$-corrections as a function of redshift. The F814W filter is similar to the $I$ band, while F606W lies between the $V$ and $R$ bands. The final rest-frame magnitudes are estimated to be accurate to ~0.2 mag, with the dominant source of error being uncertainty in the $K$-correction. The magnitudes have not been corrected for either internal or galactic extinction (which is very small for these high galactic latitude fields). The inclination, given in column (4), is calculated from the axial ratio of the outer isophotes, using $\cos^2 i = [(b/a)^2 - 0.04]/0.96$ (Rubin, Whitmore, & Ford 1988). We estimate an inclina-

TABLE 3

DERIVED PARAMETERS

| Identification Number (1) | Scale (kpc arcsec$^{-1}$) (2) | $M_B$ (mag) (3) | Inclination (4) | $r_{1/2}$ (kpc) (5) | $I_{eff}$ (mag arcsec$^{-2}$) (6) | $r_{eff}$ (kpc) (7) | $I_{cen}$ (mag arcsec$^{-2}$) (8) | $r_{disk}$ (kpc) (9) | Bulge/Disk Ratio (10) | log σ (km s$^{-1}$) (11) | [O II] EW (Å) (12) |
|---|---|---|---|---|---|---|---|---|---|---|---|
| 1..... | 5.25 | −20.8 | 24° | 5.1 | 22.9 | 2.4 | 20.7 | 3.6 | 0.20 | 2.23 (25%) | 8 (30%) |
| 2..... | 5.69 | −19.1 | 53 | 4.3 | ... | ... | 21.8 | 3.4 | 0.0 | 2.16 (30%) | 97 (50%) |
| 3..... | 6.29 | −20.0 | 35 | 4.3 | ... | ... | 21.9 | 2.9 | 0.0 | <1.96 | 89 (50%) |
| 4..... | 5.25 | −20.3 | 56 | 3.7 | ... | ... | 19.7 | 1.8 | 0.0 | 2.10 (25%) | 47 (50%) |
| 5..... | 5.25 | −21.3 | 46 | 6.9 | 20.5 | 0.8 | 20.7 | 5.1 | 0.09 | 2.08 (30%) | 9 (30%) |
| 6..... | 5.89 | −20.8 | 56 | 6.5 | 24.1 | 0.7 | 21.1 | 4.2 | 0.01 | <1.82 | ... |
| 7..... | 5.88 | −19.5 | 31 | 2.3 | ... | ... | 20.0 | 1.2 | 0.0 | <2.22 | ... |
| 8..... | 3.94 | −19.6 | 49 | 4.6 | 24.1 | 4.2 | 19.2 | 2.2 | 0.14 | 2.23 (25%) | 22 (35%) |
| 9..... | 3.02 | −18.4 | 64 | 3.7 | ... | ... | 19.3 | 2.0 | 0.0 | 2.00 (20%) | ... |
| 10 ..... | 4.15 | −19.8 | 62 | 9.1 | ... | ... | 20.1 | 3.1 | 0.07 | <1.84 | 45 (50%) |
| 11 ..... | 6.82 | −20.5 | 53 | 4.5 | 23.4 | 1.9 | 21.1 | 2.7 | 0.23 | <1.84 | 158 (50%) |
| 12 ..... | 3.54 | −20.1 | 42 | 4.1 | 21.4 | 0.7 | 20.2 | 2.7 | 0.08 | 2.21 (20%) | ... |
| 13 ..... | 6.56 | −21.1 | 53 | 4.1 | ... | ... | 20.3 | 2.6 | 0.0 | <1.83 | 17 (35%) |
| 14 ..... | 4.77 | −19.1 | 55 | 1.6 | ... | ... | 19.3 | 0.9 | 0.0 | <2.01 | 19 (30%) |
| 15 ..... | 5.74 | −20.3 | 58 | 7.3 | 24.2 | 0.9 | 21.3 | 4.1 | 0.01 | 1.93 (30%) | 31 (35%) |
| 16 ..... | ... | ... | 60 | ... | 22.9 | ... | 21.4 | ... | 0.02 | ... | ... |
| 17 ..... | 4.16 | −20.0 | ... | 2.6 | 21.3 | 2.6 | ... | ... | 1.0 | 1.91 (25%) | 9 (30%) |
| 18 ..... | 6.55 | −21.3 | 26 | 6.0 | 24.5 | 1.6 | 21.0 | 4.2 | 0.04 | 2.08 (25%) | 5 (30%) |

NOTE.—Col. (1): galaxy identification number; col. (2): physical scale of 1″ ($h = 0.75, q_0 = 0$); col. (3): total absolute $B$ magnitude corrected to zero redshift (error = 0.2 mag); col. (4): inclination (error ~10%); col. (5): half-light radius (error = 15%); col. (6): observed $I$-band brightness at effective radius (error = 0.15 mag); col. (7): effective radius of $r^{1/4}$ fit (error = 20%); col. (8): observed $I$-band disk central brightness (error = 0.15 mag); col. (9): disk scale length (error = 15%); col. (10): bulge-to-disk ratio; col. (11): corrected velocity (see text), $\sigma$ = FWHM/2.354, and total error; col. (12): rest-frame equivalent width of [O II] λ3727 and total error.

tion error in degrees of 10% for sin $i \geq 60°$ and 15% for sin $i < 60°$. Galaxy sizes and brightnesses (cols. [5]–[9]) are derived from the F814W ($I$) band images, so as to minimize the effects of obscuring dust and young star formation. The half-light radius measured following the method of Phillips et al. (1995b) gives a *model-independent* measure of the galaxy light profile. Fitting the $I$-band surface brightness profile with $r^{1/4}$ and/or exponential disk profile allows us to derive bulge and disk model parameters. We have adopted errors of 0.15 mag in the surface brightnesses and 15% in the length scales (20% for the effective radii, $r_{\rm eff}$, as it is somewhat less reliable) based on the simulations of Phillips et al. (1995a). Column (10) gives the bulge-to-disk ratio from the profile fits. Column (11) gives the emission-line velocity width in terms of sigma ($\sigma$ = FWHM/2.35) of the Gaussian. These final velocities have been corrected for instrumental broadening, $(1 + z)$ redshift effect, sin $i$ inclination and spatial extent of the spectrum (see § 4.6). The quoted error includes an estimate from these different sources but is dominated by the error in fitting a Gaussian profile to the emission line. For the single elliptical galaxy in our sample, we only made corrections for instrumental and redshift effects. The [O II] equivalent width, in column (12), is corrected for redshift. Here the error is dominated by the uncertainty in determining the continuum level of the emission line.

The 17 galaxies with redshifts range from $z = 0.205$ to 0.837. The absolute $B$ magnitudes listed in Table 3 range from $M_B = -18.4$ to $-21.3$. For comparison, an $L^*$ galaxy has $M_B = -20.1$. Thus, our sample ranges from about 1.5 mag fainter than $L^*$ to about 1.5 mag brighter than $L^*$.

## 4. DISCUSSION

### 4.1. *Is Our Sample Representative of Faint Field Galaxies?*

As mentioned above, the galaxies for which we have obtained spectra come from a larger $I < 22$ magnitude-limited sample, which is being studied for its structural and photometric properties (e.g., Forbes et al. 1994). Selection effects are crucial if one is studying galaxy distributions (e.g., number counts), but less so when comparing intrinsic properties of individual galaxies, as done in this paper. Nevertheless, we still wish to know whether our sample is representative of faint field galaxies.

The median redshift of our sample is $\bar{z} \sim 0.48$. The ground-based $I < 22$ redshift surveys of Lilly et al. (1995) and Tresse et al. (1993) find a median redshift of $\bar{z} \sim 0.6$, i.e., roughly comparable to that of our sample. In Figures 5 and 6, we compare the color and half-light radius to the somewhat larger sample of Phillips et al. (1995b). Phillips et al. confirmed that their WFPC2 selected sample was essentially 100% complete, over a small sky area area, to $I < 21.7$. Of their 64 galaxies, three are in common with our sample. In comparing the total $V-I$ color versus total $I$ magnitude, we find that our sample has a similar distribution in $V-I$ color to that of Phillips et al. between $I = 19$ and 21, but at fainter magnitudes we may be systematically biased against the reddest galaxies (see Fig. 5). These galaxies tend to be the bulge-dominated systems. Next, we compare the half-light radii from Phillips et al. with our sample in Figure 6 and find little difference.

Finally, we examine the morphological mix of our sample. Morphological types from WFPC2 are available for 200 galaxies in Forbes et al. (1994). This sample is essentially complete to $I < 22$. Of the 203 galaxies, 10 are in common with our current sample. Figure 7 shows that the late-type galaxies are fairly well represented in our current sample, but we seem to be deficient in early-type/bulge-dominated galaxies relative to the large magnitude-limited sample (as suggested by the $V-I$ color distribution). As we separate bulge-dominated galaxies from the analysis that follows, this difference in morphological mix should not affect our conclusions. Although our sample is small and in no way complete, it appears to be a reasonably fair and representative sample of field disk galaxies with $I < 22$.

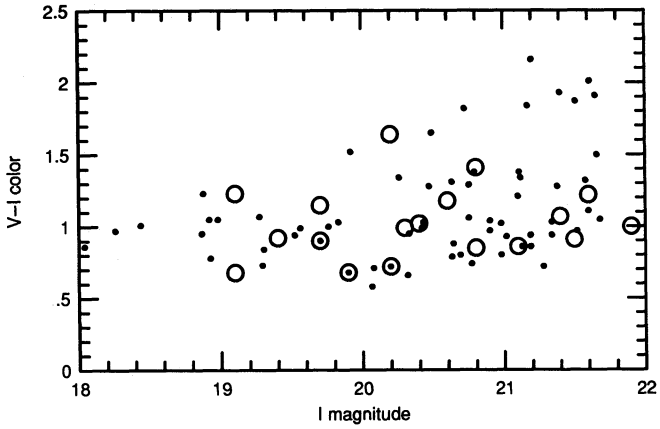


FIG. 5.—Total $V-I$ color vs. total $I$-band magnitude. The magnitude-limited WFPC2 sample ($I < 21.7$) of Phillips et al. (1995b) is shown as small circles, and our sample is shown as large open circles. Three galaxies are common to both samples. Errors on individual measurements are ~0.15 mag. Both our sample and that of Phillips et al. have a median color of 1.0. For comparison purposes, a typical local Sbc spiral has rest-frame $V-I$ color 1.1 (Frei & Gunn 1994).

### 4.2. *The Elliptical Galaxy*

Our sample contains one example of a bulge-dominated galaxy (number 17). Although we have classified it as an elliptical we cannot rule out the presence of a weak disk (i.e., it could be an S0 galaxy). Visually, the galaxy reveals asymmetric isophotes. The inner parts of the surface brightness profile are well fit by a pure $r^{1/4}$ law (see Fig. 2). We derive an $r^{1/4}$ effective radius that is the same as the half-light radius (2.6 kpc). This value can be compared to nearby ellipticals using the size-luminosity relation found by Bing-

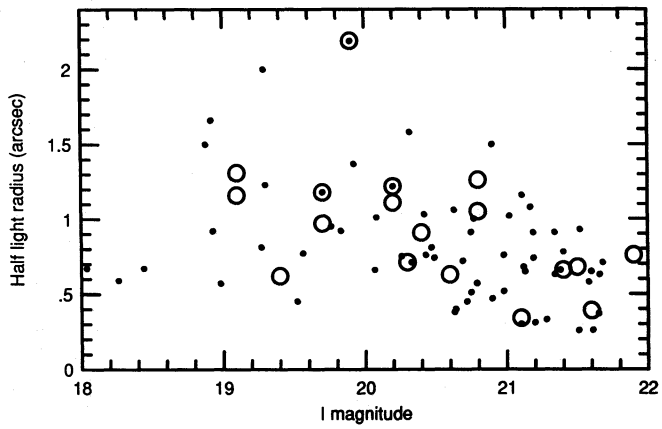


FIG. 6.—Angular half-light radius vs. total $I$-band magnitude. Symbols are the same as in Fig. 5. Errors on individual measurements are 0.15%. Our sample has a median half-light radius of 0.″9, whereas it is 0.″75 for the Phillips et al. (1995b) sample.

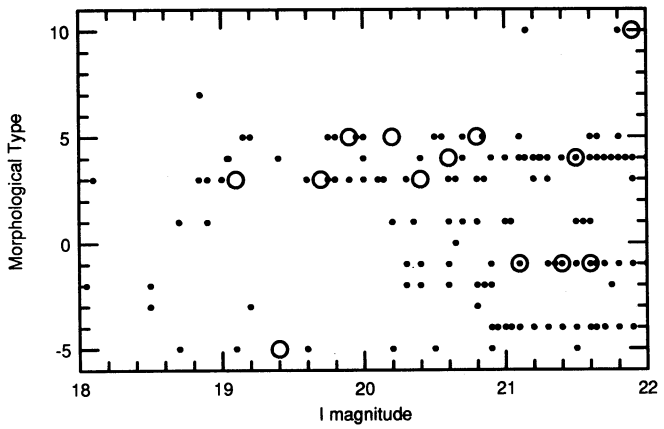


FIG. 7.—Morphological type vs. total $I$-band magnitude. The magnitude-limited WFPC2 sample of Forbes et al. (1994) is shown as small circles. This sample is 70% complete to $I = 22$ and essentially 100% complete to $I = 21$. Our current sample is shown by large open circles. There are 10 galaxies in common. Here $E = -5$, E/S0 $= -3$, S0 $= -2$, S0/a $= 0$, Sa $= 1$, Sb $= 3$, Sc $= 5$, Sd $= 7$, Irregulars $= 10$, bulge dominated $= -4$, intermediate $= -1$, and disk dominated $= 4$. Barred spirals are included with their spiral subtype; double nucleus galaxies are not shown.

geli, Sandage, & Tarenghi (1984). On this basis, we would predict an effective radius, if it followed the local scaling relation, of 2.2 kpc (using $H_0 = 75$). This agrees with the measured effective radius of $2.6 \pm 0.5$ kpc, and this is without taking into account the intrinsic scatter in the local relation. Similarly, if we use the effective radius to predict the internal velocity $\sigma$ using a projection of the fundamental plane as described by Guzman, Lucey, & Bower (1993), then we predict $\log \sigma = 2.26$. We measure an emission-line velocity width of $\log \sigma = 1.91 \pm 0.48$, which is again consistent, within the measurement errors, to that of a local elliptical with ($r_{\rm eff} = 2.6$ kpc). The absorption lines appear to have a similar velocity width.

The spectrum is interesting since, besides having the expected lines for an elliptical (i.e., Ca II H + K, the $G$ band, and Fe I $\lambda$4384), it also reveals Balmer absorption lines and [O II] $\lambda$3727 and H$\beta$ in emission. These emission lines may suggest that the galaxy has undergone a recent episode of star formation and may be a rare example of an active field elliptical (poststarburst ellipticals are usually found in clusters). We measure a total color $V-I = 0.92$, which is about 0.5 mag bluer than that predicted ($V-I \sim 1.45$) for a passive local elliptical at redshift $z = 0.324$ (Frei & Gunn 1994). The blue color could be the result of recent star formation. Thus, although this galaxy has structural parameters (i.e., $r_{\rm eff}$ and $\sigma$) similar to those expected for a local elliptical, we find evidence for some additional brightening.

### 4.3. [O II] *Equivalent Widths*

For moderate-redshift galaxies, the [O II] $\lambda$3727 line has been used by several workers as an indication of high star formation (SF) rates (e.g., Couch & Sharples 1987; Broadhurst, Ellis, & Shanks 1988). Although less accurate for quantitative studies, [O II] provides a reasonable substitute for H$\alpha$ since stellar H$\beta$ line absorption may affect H$\beta$ measurements and [O III] $\lambda$5007 is more sensitive to excitation variations (Kennicutt 1992). Other star formation diagnostics, such as Balmer absorption lines or the 4000 Å break, sample star formation over the past several Gyr.

The rest-frame [O II] equivalent widths for our sample are given in Table 3. If we divide the sample by *intrinsic* color into two bins at $B-V = 0.55$, we find that the mean equivalent width for the "red" galaxies is 19 Å, whereas the "blue" galaxies have a mean value of 59 Å. As expected, intrinsically blue galaxies have higher star formation rates. Equivalent widths greater than 20 Å suggest an SF rate of a few solar masses per year for an $L^*$ galaxy (Kennicutt 1992). We have seven such galaxies, some of which have an asymmetric visual morphology, but so do many of the galaxies with [O II] equivalent widths less than 20 Å.

### 4.4. *Physical Associations*

There are several galaxies in our sample with similar redshifts. They are numbers 6 and 7 (at $z \sim 0.595$), and 4, 5, and 1 (at $z \sim 0.477$). The former galaxies consist of a barred spiral, with a possible foreground star superposed on it, paired with a faint galaxy classified as intermediate type (see Fig. 1). Given the small projected separation of 27 kpc and the distorted outer isophotes of the spiral, it appears that the two galaxies are tidally interacting. The latter three galaxies represent a double nucleus galaxy (presumably in the late stage of a merger), and two $\sim L^*$, undisturbed spiral galaxies. The projected separation from numbers 5 to 4 is 110 kpc and 460 kpc to number 1.

We note that some apparent associations in our sample are merely projections on the sky, i.e., they appear close, with similar angular sizes, and yet they are well separated in redshift space. Such an example is shown in Figure 1 by galaxies 15 ($z = 0.566$), 16 ($z \sim 0.4$? see the Appendix), 17 ($z = 0.324$), and 18 ($z = 0.754$). Some of these galaxies show evidence for asymmetries or distortions, which might be the result of an interaction with one of the other galaxies that is projected nearby. As they are at different redshifts, this is not the case, but it does serve to highlight the risks of classifying interacting galaxies on the basis of visual appearance alone. Estimates of the frequency of interacting and merging galaxies from imaging (without knowing the redshifts of both interacting systems) are likely to be overestimated. To illustrate this, if we take the extreme view that all galaxies with asymmetries and multiple nuclei are the result of a merger or interaction (as has been done at times), then our small sample would suggest that 11 of 17 galaxies could be so classified. With redshifts and imaging data, we would reduce this to only three to four galaxies which we would consider to be clearly merging or interacting with another galaxy in the sample. This comparison does not include companion galaxies that are not in our redshift sample or evolved systems that show asymmetries but no other evidence of the secondary galaxy.

### 4.5. *Luminosity-Size Relation*

Since Freeman (1970) observed that spiral galaxies have a constant disk central surface brightness of $\mu_B = 21.65 \pm 0.3$, there has been much debate concerning the interpretation and reliability of this result. The most comprehensive study to date is that of de Jong (1995), who shows that there is no single preferred value but a range of $\mu_B$ that varies with Hubble type. He finds, for spirals (RC2 types 1–6) with semitransparent disks, that $\mu_B = 21.45 \pm 0.76$ mag arcsec$^{-2}$. We have adopted this value for the local central surface brightness, which can be expressed in terms of a local luminosity-size scaling relation. Assuming the total light from a pure exponential disk is $L_T = 2\pi\theta_d^2 L_0$, where $\theta_d$ is the angular disk scale length and $L_0$ is the central surface brightness (in $L_\odot$ arcsec$^{-2}$), we can derive the local

luminosity-disk size scaling relation to be

$$\log (r_d/\mathrm{kpc}) = -0.2\ M_{B,\mathrm{disk}} - 3.42(\pm 0.15)\ .$$

We have calculated the disk magnitude ($M_{B,\mathrm{disk}}$), for our sample by subtracting the light in the bulge (<0.2 mag in all cases) from the total magnitude in Table 3. We have not made any correction for inclination or internal absorption (which tend to largely cancel each other in calculating face-on surface brightnesses).

In Figure 8 we show the physical disk scale length against rest frame absolute $B$ magnitude of the disk for our sample galaxies and the local scaling relation for spirals. Most of our sample galaxies fall slightly below the mean relation, i.e., to smaller scale lengths and/or to brighter magnitudes. A linear regression fit, inversely weighted by the error in disk scale length gives

$$\log (r_d/\mathrm{kpc}) = -0.15 \pm 0.05\ M_{B,\mathrm{disk}} - 2.58 \pm 1.0\ .$$

Thus, our sample is offset to lower scale lengths with a flatter slope, but with formal errors that are consistent with the local relation. If we fix the slope to a value of $-0.2$, then the change in the other coefficient relates to a change in central surface brightness only. This gives a brightening of 0.85 mag, corresponding to $\mu_B = 20.6 \pm 0.2$ mag arcsec$^{-2}$ for the sample as a whole. We note that surface brightnesses are unaffected by changes in $q_0$. If we restrict our sample to just those that are clearly spiral in nature (filled symbols in Fig. 8), then both the slope and intercept are closer to the local relation values. Again for a fixed slope, the spirals are brightened by $\Delta\mu_B \sim 0.6$ mag, giving $\mu_B = 20.9 \pm 0.1$. Thus, our sample suggests that deviations from the local scaling relation are strongest in the very late-type/irregular galaxies (although in some cases this is probably because the disk scale length is poorly defined). Schade et al. (1995) have recently examined the luminosity-size relation for 32 galaxies with redshifts $0.5 < z < 1.2$. Scale lengths have been measured from WFPC2 images and redshifts obtained from CFHT spectra. They find a value of $\mu_B = 20.3 \pm 0.2$ for galaxies with obvious spiral structure and find no statistical difference between these spirals and the small featureless objects or irregulars. However, they also note the difficulty of quantifying the meaning of a disk scale length for the small and irregular galaxies. Their data for more distant galaxies ($\bar{z} \sim 0.75$) suggest a brightening of $\Delta\mu_B \sim 1.2$ mag, i.e., slightly higher than our estimate for $\bar{z} \sim 0.5$ galaxies. When we divide our sample into intrinsically blue and red galaxies at $B-V = 0.55$ (circles and triangles, respectively, in Fig. 8), we find $\mu_B = 20.8 \pm 0.3$ for the blue galaxies and $\mu_B = 20.4 \pm 0.3$ of the red galaxies. Although the errors are large, there is an indication that the blue galaxies deviate less from the local relation than do the red galaxies. It is possible that star formation has conspired to move points parallel to the local relation, i.e., low-luminosity systems may have star formation preferentially in their outer parts, so that the brightening is accompanied by an increased scale length. If this were the case, we might expect the higher luminosity galaxies in our sample to be dominated by blue galaxies, which is not seen.

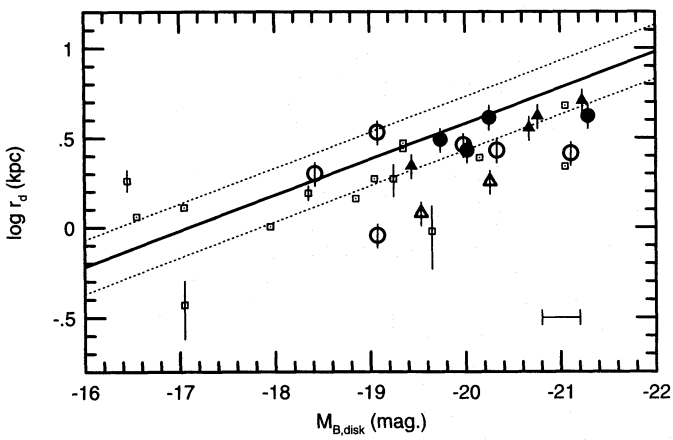


FIG. 8.—Luminosity–disk size relation. The exponential disk scale length is plotted against rest-frame absolute $B$ magnitude of the disk. Filled symbols represent galaxies that are clearly spiral in nature, and open symbols represent other galaxies. The sample is also divided by intrinsic color, with circles for blue galaxies and triangles for red galaxies. Errors are estimated to be 15% in the scale length and 0.2 mag in absolute magnitude. The magnitude error bar is shown in the lower right. Galaxies from the $\bar{z} \sim 0.3$ sample of Colless et al. (1994) are shown by small open squares. The solid and dashed lines represent the local relation assuming a central surface brightness of $21.45 \pm 0.76$ $B$ mag arcsec$^{-2}$ (see § 4.5).

Additional support for the modest brightening of distant field galaxies comes from the ground-based study of Colless et al. (1994). Their sample is at a slightly lower median redshift ($\bar{z} \sim 0.3$) than ours but contains a comparable number of galaxies. Their seeing was sub-arcsecond (0.″5–1.″0), but it was not sufficient for a direct visual classification of the galaxy's morphological type. Furthermore, they could not decompose the surface brightness profiles into bulge and disk combinations, as we have done. With the limited number of resolution elements, they were only able to fit either a disk *or* a bulge profile. This will introduce a small bias toward smaller scale lengths for early-type spirals. They measured a total of 19 galaxy scale lengths and seven upper limits. After excluding the two bulge-dominated systems, we also show their data in Figure 8 (after correcting to $H_0 = 75$ km s$^{-1}$ Mpc$^{-1}$ and $q_0 = 0$). Their data also follow the same general trend as ours, slightly below the local relation and with a flatter slope. A similar conclusion (that disk galaxy sizes have evolved little) was reached by studying somewhat brighter, less distant ($\bar{z} \sim 0.2$) field galaxies from WFPC1 imaging (Mutz et al. 1994; Phillips et al. 1995a).

We conclude that *spiral galaxies at moderate redshift follow a similar luminosity-size relation to local galaxies, albeit with a modest brightening of ~1 mag.*

### 4.6. *Luminosity-Velocity Relation*

Next we examine the relationship between a galaxy's internal velocity and its total luminosity, and we compare it to those of local galaxies. There does not yet exist a systematic and complete sample of local field galaxies studied by their internal velocity properties. Most studies of the Tully-Fisher relation have concentrated on well-behaved, noninteracting, nonbarred galaxies so as to reduce the scatter about the relation for distance-determination purposes. In Figure 9 we show the local scaling relations of Rubin et al. (1985) for normal (i.e., noninteracting, nonbarred) field spirals. Their $V_{\mathrm{max}}$ of the rotation curve has been converted into $\sigma$ of a Gaussian assuming that the FWHM of the Gaussian represents the full range in internal velocity, i.e., $\sigma = 2 \times V_{\mathrm{max}}/2.35$. This is roughly analogous to integrated H I velocity widths, $W_{50}$. The Rubin et al. relations are derived from H$\alpha$ rotation curves and have a dispersion of ~0.5 mag per Hubble type. The H I–derived Tully-Fisher

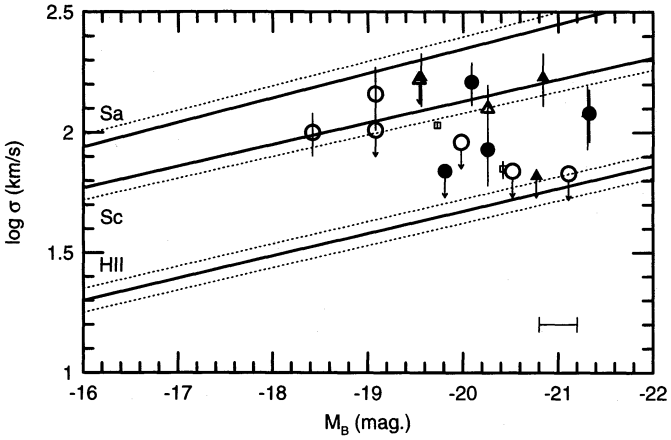


FIG. 9.—Luminosity–interval velocity relation. The velocity line width sigma ($\sigma = 2V_{max}/2.35$) is plotted against total absolute $B$ magnitude of the galaxy. The same symbols are used as in Fig. 8. Two disk-dominated galaxies ($z \sim 0.2$) from Vogt et al. (1993) are shown by small open squares. The upper solid lines represent the local relation for Sa and Sc galaxies from Rubin et al. (1985), with dashed lines giving the upper and lower bounds. The H I Tully-Fisher relation would lie between Sa and the Sc galaxy relations. The lower lines represent the local relation for H II galaxies from Telles (1995).

relation (e.g., Pierce & Tully 1988) falls between the Rubin et al. Sa and Sc galaxy relations. We would expect Sd/Irr galaxies, with a lower velocity for a given luminosity, to lie slightly below the Rubin et al. relation for Sc spirals. The measured velocity width in barred galaxies will depend on the relative orientation of the bar and slit. We also show in Figure 9 the local relation for H II galaxies from Telles (1995). Such galaxies are dominated by a global starburst and have $M_B$ up to $-21.0$ (Telles & Terlevich 1993). The internal velocities for the H II galaxies are derived from Hα emission-line widths. Thus, at a given luminosity, there will be a large range of internal velocities for a sample of randomly selected local field galaxies, unlike disk size, which reveals a relatively tight relationship with luminosity.

By using local relations that are determined from ionized gas, we will avoid any systematic differences from those derived using neutral hydrogen gas. However, we must assume that the spatial distribution of [O II], Hβ, and [O III] derived velocities are similar to that of Hα. In Figure 9, we express internal velocity in terms of σ of the Gaussian (=FWHM/2.35) from the emission-line widths. Gaussians are a good approximation to the emission-line profiles. After measuring the emission-line velocity widths, we have made the usual corrections for instrumental broadening, redshift effect, and inclination.

As our galaxies tend to be somewhat larger than the slit width, the orientation of the slit is important. Thus, we need to make an additional correction for the limited spatial coverage of the slit along the galaxy's major axis. The measured velocity needs to be increased if the spatial extent of the spectrum does not probe to sufficiently large galactocentric radii in order to reach each galaxy's maximum rotation velocity ($V_{max}$). Fortunately, galaxy rotation curves are relatively flat beyond the central regions, and so any corrections are small. This effect can be quantified crudely using the parameterization of local galaxy rotation curves found by Persic & Salucci (1991), based on the fact that outer rotation curve gradients vary systematically with galaxy luminosity. They found the radial dependence of rotation velocity to be

$$\frac{V(r)}{V_{max}} = 1 + \left(0.12 - 0.24 \log \frac{L_B}{L_{B*}}\right)\left(\frac{r}{2.2r_d} - 1\right).$$

We recognize that using this relation assumes that distant galaxies have similar rotation curve forms to local galaxies, but as this correction is typically ~8% for our sample, it does not affect the general conclusions. The larger corrections are applied to those few galaxies with slits close to the minor axis. Such galaxies in our sample tend to have velocity upper limits. The final corrected velocities are listed in Table 3.

For two of our galaxies, the emission lines of Hβ and [O II] are extended by about 10 pixels from the spectrum centroid, thus allowing us to derive spatial velocity information, or rotation curves, and hence to measure $V_{max}$ directly for comparison with the velocity derived from emission line widths. The two galaxies (4 and 5) are a double nucleus system and a regular-looking Sb spiral, both at redshift $z \sim 0.48$. Applying the same redshift and inclination corrections, and assuming $\sigma = 2 \times V_{max}/2.35$, the rotation curves give a σ value of $\log \sigma = 2.11$ and $\log \sigma = 2.23$ for galaxies 4 and 5, respectively. In Table 3, we give values of $2.10 \pm 25$ and $2.08 \pm 30$, respectively. Thus, the emission-line velocity widths are similar to, but perhaps slightly lower than, those derived from the emission-line rotation curves. A full description of the rotation curve derivation for these galaxies, and others from a different study, will be presented by Vogt, Forbes, & Phillips (1995).

We find that our sample galaxies fill the region between local Sa and H II galaxies. Most of the spiral galaxies are barely consistent with the Sc galaxy relation. If we take the six spirals with detections, and the same slope as the Rubin et al. relation, we find that the brightening is $\Delta M_B \sim 0.4$ mag with respect to the Sc relation. Of the galaxies that lie close to the H II galaxy relation, most of these have intrinsic blue colors, often with very high [O II] equivalent widths (i.e., they are likely to be starbursts). One exception is the barred spiral (number 6) for which the slit was placed directly along the bar, which may have led to a systematically lower velocity width (van Albada & Roberts 1981). The starbursting galaxies may be similar to the moderate-redshift compact narrow emission-line galaxies (CNELGs) described by Koo et al. (1995a), which they showed are equivalent to luminous examples of local H II galaxies. The presence of a starburst could lead to a systematically lower emission-line width if a small number of low-velocity star-forming complexes (giant H II regions) dominate the ionized gas in the central regions. In this case, the line width could have a significant contribution from the internal motion induced by stellar energy release within the H II regions. Some support for this comes from Telles & Terlevich (1993), in which they find that H II galaxies may have emission-line widths that are up to a factor of 2 (0.3 in the log) smaller than those derived from H I 21 cm measurements. Other possibilities also remain, such as a small spatial extent for the optical data compared to the H I data. These effects would move points diagonally to the lower right in Figure 9.

We also plot data for two disk systems from Vogt et al. (1993), after converting their $R$-band magnitudes (Vogt 1995) to $M_B$ using the Frei & Gunn (1994) tables and assuming both to be late-type spirals (they did not have the

benefit of *HST* imaging). The first galaxy ($z = 0.211$) is described as "elongated with a small bulge" and has very strong emission lines. It lies just above the H II relation in Figure 9. The second ($z = 0.201$) is an "elongated" cluster galaxy, presumably also a spiral, that lies close to the relation for Sc galaxies. These two galaxies lie within the locus of our sample and are also consistent with some brightening relative to local galaxies.

In summary, we find that our moderate-redshift field galaxies fall within the region defined by local spirals and H II galaxies in terms of their internal velocities. Many of the spiral galaxies in our sample lie close to the local relation for Sc galaxies, with only modest brightening. However, a sizable fraction of the sample lies closer to the local relation for H II galaxies. These galaxies tend to be starbursting galaxies, as indicated by their blue colors and high [O II] equivalent widths. For these galaxies, it is important to check the emission-line velocity widths against those determined directly from rotation curves. So although our luminosity-velocity relation does not provide us with such a clear-cut interpretation as the luminosity-size relation, it does suggest that some fraction of moderate-redshift galaxies have velocity widths characteristic of local galaxies with $\sim 1$ mag of brightening.

### 4.7. *The Nature of the Faint Blue Galaxies*

One of the major outstanding puzzles of cosmology is the nature of the blue galaxies that appear to dominate the number counts, by a factor of 3–5 above nonevolution predictions, by $B \sim 23$. For example, Cowie et al. (1991) presented redshifts for 22 galaxies with $B \leq 24$ and claimed that counts at these magnitudes were "...dominated by a population of small blue galaxies..." that is not seen locally. The current explanations for these blue galaxies include (1) an entirely new population at moderate redshifts that has disappeared by today (Cowie et al. 1991; Babul & Rees 1992), (2) mergers and associated star formation that have distorted the galaxy luminosity function compared to that at the present epoch (Broadhurst et al. 1992), or (3) the possibility that uncertainties in the local galaxy luminosity function are not known well enough to require alternative explanations yet (Koo & Kron 1992). The first two of these scenarios would predict that there exists a *large* population of galaxies at moderate redshift that have "disappeared" by the present epoch and thus do not have local counterparts.

Recently, Cowie et al. (1995) have presented deep WFPC2 F814W images of faint field galaxies. The main result of their paper is the identification of a completely new morphological class of galaxy called "chain galaxies." These galaxies are fainter than our magnitude limit of $I = 22$ and are very blue with a linear, beaded morphology. Cowie et al. suggests that they have redshifts $z \sim 1.5$. If spectra are obtained for these galaxies, it will be useful to compare their properties with the luminosity-size and luminosity–internal velocity relations to assess their true nature.

As discussed in § 4.2, our sample, although small, appears to be representative of disk galaxies at $B \sim 23$, i.e., the regime of the faint blue galaxy excess. If the excess is a factor of 3–5 above nonevolutionary predictions (Cowie et al. 1991), then we would expect about 75% or 13–14 galaxies in our sample to belong to such an excess population. What, then, can we say about such galaxies from our sample? By examining their disk sizes and internal velocities, we find that many of our sample galaxies show evidence for modest ($\Delta M_B \sim 1$ mag) evolutionary brightening relative to the present epoch but otherwise have quantitative parameters that are similar to the local scaling relations. The single bulge-dominated galaxy in our sample appears to be structurally similar to local ellipticals but is $\sim 0.5$ mag bluer than expected for a passive local elliptical and reveals weak emission lines. Our general findings are supported by the WFPC2 study of Phillips et al. (1995b), which is complete to $I < 21.7$ ($B < 24$) and finds that the angular size versus apparent magnitude relationship is consistent with mild luminosity evolution of the local galaxy populations. As our sample is small, it is premature to draw strong conclusions regarding the nature of faint galaxy evolution. Nevertheless, we do not see evidence for a dominant population of galaxies at moderate redshift that have no local counterparts, once a modest amount of fading has occurred. This is consistent with the recent results from deep surveys of Lilly et al. (1995).

## 5. CONCLUDING REMARKS

In the near future, we expect many new data to address the issue of galaxy sizes and internal kinematics at moderate redshift, using the more efficient multislit mode of the LRIS spectrograph on the Keck telescope (e.g., Koo et al. 1995b) and with the AUTOFIB multifiber instrument on the Anglo-Australian Telescope (Rix, Guhathakurta, & Colless 1995). The combination of full rotation curves and surface brightness profiles will allow us to examine the radial dependence of mass and $M/L$ in these distant galaxies (e.g., Persic & Salucci 1990; Forbes 1992). With larger samples, and thus better statistics, additional aspects of faint galaxy evolution can be addressed, such as the morphology-density relation at moderate redshift, clustering properties of field galaxies, and the change in galaxy properties with redshift.

In summary, for a small but representative sample of moderate redshift ($0.2 < z < 0.84$) field galaxies, we present spectra from the Keck telescope and imaging from the *HST* WFPC2. From these data, we have derived various quantitative physical parameters, including scale lengths from surface brightness profiles and internal velocities with a resolution of $\sigma = 55$–$80$ km s$^{-1}$. We examine the relationship between galaxy luminosity and both disk scale length and internal velocity. Together, these data suggest that many spiral and disk galaxies with redshifts $\sim 0.5$ have undergone modest $\Delta M_B \sim 1$ mag luminosity evolution. Otherwise, they have values characteristic of local galaxies. The single elliptical galaxy in our sample has structural parameters (i.e., $r_{\rm eff}$ and $\sigma$) consistent with those for a local elliptical but is much bluer in the rest frame than expected for a passive elliptical. Although we have found evidence for mild luminosity evolution at moderate redshifts, we *do not* see evidence for dominant population of galaxies that has completely disappeared by the present epoch, as suggested by some galaxy evolutionary scenarios.

We thank S. Faber, R. Guzmán, T. Bida, and the Keck Observatory staff for help with the observations, and N. P. Vogt, G. Wirth, and P. Guhathakurta for useful discussions. We also thank the referee for many helpful comments. This research was funded by grants GO-2684.04-87A, GO-2684.04-87A, AST 91-20005, and AST 88-58203.

## APPENDIX

## INDIVIDUAL GALAXIES

1. *030505.0−001143.*—This is a good example of a near face-on spiral at redshift 0.477. It obeys both the luminosity-disk size and luminosity–velocity width scalings for local galaxies.

2. *030504.9−001138.*—Although projected on the sky close to galaxy 030505.0−001143, it is at a higher redshift. This galaxy is a late-type galaxy with an extremely high rest-frame [O II] equivalent width, i.e., currently undergoing a burst of star formation. It is the faintest galaxy in our sample with $I = 21.9$. It is interesting to note that this galaxy has fairly similar half-light radius to galaxy number 1, and yet one would expect that they have quite different values from examining Figure 1 by eye. This is largely because of the 2 mag difference in surface brightness of the two objects, which is not obvious in the image.

3. *030501.3−001039.*—We chose this galaxy based on its peculiar morphology and its unknown nature (Glazebrook et al. 1994 suggested either a super-starburst galaxy or a gravitational lens). The redshift was known from the work of Glazebrook et al. (the only one in our sample). The spectrum, from the main part of the lower ring, supports the starburst origin with strong, unresolved lines typical of an H II region and a large [O II] equivalent width. Examination of the two-dimensional spectrum suggests that there is small velocity shift across the system, making the gravitational lens interpretation less likely. The disk scale length and surface brightness are less reliable for this peculiar galaxy than for others.

4. *030458.0−001135.*—This galaxy shows a clear double nucleus, separated by $\sim 1\farcs0$ (5.3 kpc), and it is presumably in the late stage of a merger. The measured line width reflects the two velocity components. An exponential fit was made to the isophotes giving $r_{\rm disk} = 1.8$ kpc, but the scale size is not very meaningful in this case.

5. *030459.2−001146.*—At the same redshift as the double nucleus galaxy ($z = 0.477$). It has a high luminosity ($M_B = -21.3$) and has the largest disk scale length ($r_{\rm disk} = 5.1$ kpc) in our sample.

6. *030503.4−001010.*—We classified this galaxy as a barred spiral. The photometry is somewhat uncertain, as we have attempted to exclude the possible foreground star which lies just off the nucleus. The slit is parallel to the galaxy bar, so in this case we may have a significant contribution from noncircular motions.

7. *030503.3−001015.*—This galaxy appears to be a physical companion of the barred spiral (030503.4−001010), since both have a redshift of $\sim 0.595$ and a separation of 27 kpc. The morphological type is somewhat uncertain; we have classified it as an intermediate type, but the surface brightness profile is well fit by a single exponential disk.

8. *010958.5−022724.*—We have classified this galaxy as an asymmetric Sb, as its appearance is clearly distorted from a typical Sb spiral. It has a relatively high velocity width and [O II] equivalent width.

9. *010958.1−022740.*—This is the closest galaxy in our sample (with a redshift of 0.205) and the least luminous. It appears to be undergoing a merger or interaction with a small galaxy, and so we have classified it as a double nucleus system.

10. *010957.4−022807.*—This galaxy has a low surface brightness and appears to show a spiral arm structure. It is very blue with strong [O II] emission, suggesting recent star formation.

11. *171220.8+333559.*—At a redshift of 0.837, this is the most distant galaxy in our sample. It is also extreme in its rest-frame [O II] equivalent width ($\sim 150$ Å). Visually, it appears to be asymmetric.

12. *171221.4+333556.*—This is a nearby ($z = 0.256$), asymmetric, and blue Sb spiral. Its luminosity is close to $L^*$. The [O II] $\lambda 3727$ line is blueward of our wavelength coverage, but the visual morphology and blue color suggest a recent burst of star formation across the disk.

13. *171227.1+333549.*—Images of this galaxy show distortions with a possible faint companion. The galaxy is distant ($z = 0.759$) and luminous ($M_B = -21.1$).

14. *171227.0+333558.*—The morphological type of this galaxy is somewhat uncertain; we have classified it as an intermediate type, but the surface brightness profile is well fit by a single exponential disk. The galaxy is also quite blue.

15. *171229.5+333626.*—In this case, the slit lies close to the minor axis of the galaxy, and a fairly large correction to the measured velocity width was required. The image suggests spiral arms and ongoing star formation. The luminosity ($M_B = -20.3$) and scale length ($r_{\rm disk} = 4.1$ kpc) are close to $L^*$ and the average disk scale length for local galaxies of 3.5 kpc quoted by Mutz et al. (1994).

16. *171229.5+333634.*—We have not managed to determine a convincing redshift for this galaxy (the only one in our sample without a redshift). Comparing the angular half-light radius and apparent $I$ magnitude with the latest mild luminosity evolution models of Gronwall & Koo (1995) suggests that $z \sim 0.4$. This is consistent with a 4000 Å break in the spectrum at $\sim 5600$ Å. The resulting absolute magnitude $M_B = -18.9$ would place it at the low-luminosity end of our sample. The galaxy shows evidence for a weak bar along the major axis, and the outer isophotes are clearly distorted, suggesting an interaction, possibly with a faint companion just visible in Figure 1.

17. *171229.3+333636.*—This is the only clear case of a bulge-dominated galaxy in our sample ($z = 0.324$), and it has been discussed in detail in § 4.2.

18. *171229.9+333644.*—Close to face-on, this galaxy shows asymmetric structure and possible off-nucleus star formation. The rest-frame [O II] equivalent width is 34 Å. It is a highly luminous ($M_B = -21.3$), distant ($z = 0.754$) galaxy.

REFERENCES


Babul, A., & Rees, M. J. 1992, MNRAS, 255, 346
Binggeli, B., Sandage, A., & Tarenghi, M. 1984, ApJ, 304, 305
Broadhurst, T., Ellis, R. S., & Glazebrook, K. 1992, Nature, 355, 55
Broadhurst, T., Ellis, R. S., & Shanks, T. 1988, MNRAS, , 235, 827
Colless, M. M., Schade, D., Broadhurst, T. J., & Ellis, R. S. 1994, MNRAS, 267, 1108
Couch, W. J., Ellis, R. S., Sharples, R. M., & Smail, I. 1994, ApJ, 430, 121
Couch, W. J., & Sharples, R. M. 1987, MNRAS, 229, 423
Cowie, L. L., Hu, E. M., & Songaila, A. 1995, ApJ, 110, 1576
Cowie, L. L., Songaila, A., & Hu, E. M. 1991, Nature, 354, 400
de Jong, R. S. 1995, Ph.D. thesis, Univ. Groningen
Dressler, A., Oemler, A., Butcher, H. R., & Gunn, J. E. 1994a, ApJ, 430, 107
Dressler, A., Oemler, A., Sparks, W. B., & Lucas, R. A. 1994b, ApJ, 435, L23
Faber, S. M., & Jackson, R. E. 1976, ApJ, 204, 668
Forbes, D. A. 1992, A&AS, 92, 583
Forbes, D. A., Elson, R. A. W., Phillips, A. C., Koo, D. C., & Illingworth, G. D. 1994, ApJ, 437, L17
Franx, M. 1993a, ApJ, 407, L5
———. 1993b, PASP, 105, 1058
Freeman, K. 1970, ApJ, 160, 811
Frei, Z., & Gunn, J. E. 1994, AJ, 108, 1476
Giraud, E. 1992, A&A, 257, 501
Glazebrook, K., Lehar, J., Ellis, R., Aragon-Salamanca, A., & Griffiths, R. 1994, MNRAS, 270, L63
Griffiths, R. E., et al. 1994a, ApJ, 437, 67
———. 1994b, ApJ, 435, L19
Gronwall, C., & Koo, D. C. 1995, ApJ, 440, L1
Guzmán, R., Lucey, J. R., & Bower, R. G. 1993, MNRAS, 265, 731
Kennicutt, R. C. 1992, ApJ, 388, 310
Koo, D. C., Guzmán, R., Faber, S. M., Illingworth, G. D., Bershady, M. A., Kron, R. G., & Takamiya, M. 1995a, ApJ, 440, L49
Koo, D. C., & Kron, R. G. 1992, ARA&A, 30, 613
Koo, D. C., et al. 1995b, in preparation
Lavery, R. J., Pierce, M. J., & McClure, R. D. 1992, AJ, 104, 2067
Lilly, S. J., et al. 1995, preprint
Mutz, S., et al. 1994, ApJ, 434, L55
Oke, J. B., et al. 1995, PASP, 107, 375
Persic, M., & Salucci, P. 1990, ApJ, 247, 349
———. 1991, ApJ, 368, 60
Phillips, A. C., Bershady, M. A., Forbes, D. A., Koo, D. C., Illingworth, G. D., Reitzel, D. B., Griffiths, R. E., & Windhorst, R. A. 1995a, ApJ, 444, 21
Phillips, A. C., et al. 1995b, in preparation
Pierce, M. J., & Tully, R. B. 1988, ApJ, 330, 579
Rix, H. W., Guhathakurta, P., & Colless, M. M. 1995, in preparation
Rubin, V. C., Burstein, D., Ford, W. K., & Thonnard, N. 1985, ApJ, 289, 81
Rubin, V. C., Whitmore, B. C., & Ford, W. K. 1988, ApJ, 333, 522
Schade, D., Lilly, S. J., Crampton, D., Hammer, F., Le Fevre, O., & Tresse, L. 1995, preprint
Telles, E. 1995, personal communication
Telles, E., & Terlevich, R. 1993, Ap. Space Sci., 205, 49
Tresse, L., Hammer, F., Le Fevre, O., & Proust, D. 1993, A&A, 277, 53
Tully, R. B., & Fisher, R. 1977, A&A, 54, 661
van Albada, G. D., & Roberts, W. W. 1981, ApJ, 246, 740
Vogt, N. P. 1995, private communication
Vogt, N. P., Forbes, D. A., & Phillips, A. C. 1995, in preparation
Vogt, N. P., Herter, T., Haynes, M. P., & Courteau, S. 1993, ApJ, 415, L95